RSC Advances

This article can be cited before page numbers have been issued, to do this please use: P. Ledwon, N. Thomson, E. Angioni, N. J. Findlay, P. Skabara and W. Domagala, *RSC Adv.*, 2015, DOI: 10.1039/C5RA06993A.

ROYAL SOCIETY OF CHEMISTRY

www.rsc.org/advances

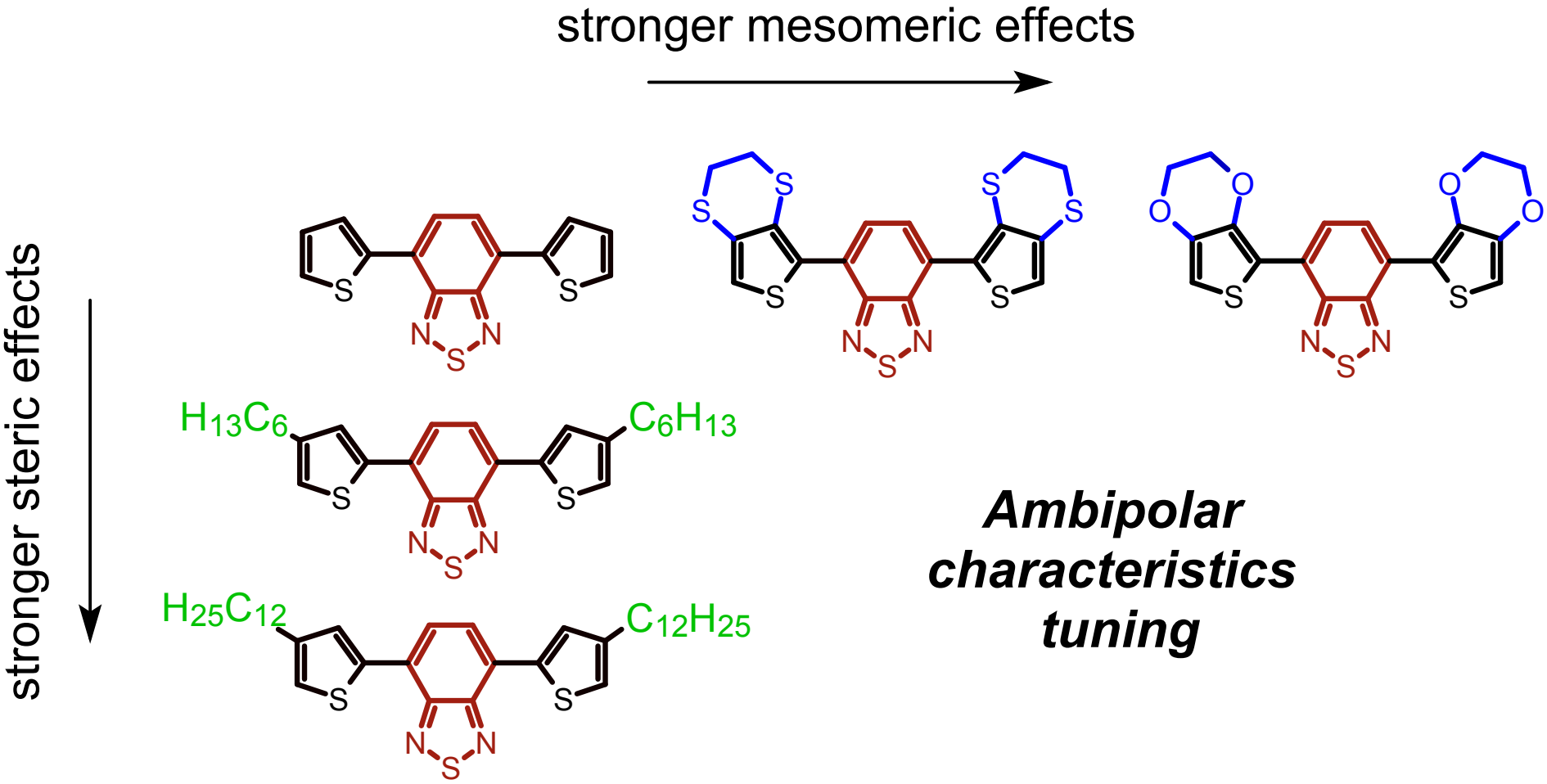

View Article Online
DOI: 10.1039/C5RA06993A

Journal Name

ARTICLE

The role of structural and electronic factors in shaping the ambipolar properties of donor-acceptor polymers of thiophene and benzothiadiazole†

Received 00th January 20xx,
Accepted 00th January 20xx

DOI: 10.1039/x0xx00000x

www.rsc.org/

Przemyslaw Ledwon [a], Neil Thomson [b], Enrico Angioni [b], Neil J. Findlay [b], Peter J. Skabara [b] and Wojciech Domagala [a,*]

The influence of different thiophene donor units on electrochemical and spectroscopic properties of benzothiadiazole based donor-acceptor π-conjugated organic materials is studied. Two different structure modification vectors of the donor units are being considered – one addressing the intermolecular interactions through off-conjugation side chain architecture, and the other focusing on intramolecular interactions tuned by in-conjugation substituents. Electrochemical and simultaneous *in situ* EPR-UV-Vis-NIR spectroelectrochemical studies of the oxidative (p-) and reductive (n-) doping processes, which are responsible for the optoelectronic properties of these materials, revealed their disparate course and dissimilar effects of redox reactions of the conjugated π-bond. While p-doping prevalent species were found to comprise intensively interacting spin bearing and spinless charge carriers, the n-doping state was found to involve only one type of negatively charged carrier, with spin carrying species being selectively generated at due cathodic potentials. No spin pairing of these negative polarons was observed with their increasing population behaving like a collection of localised charge carriers. Qualitative and quantitative comparisons between the p- and n-doping carrier populations provided independent support for the spin pairing phenomena of positive charge carriers. Steric effects of varying alkyl side chain substitution have demonstrated predominant impact on the electrochemical properties of investigated polymers, and, thereto related, stability of n-doped state, while mesomeric effects of different 3,4-ethylenechalcogenide thiophene functionalities have been found to shape the energy level related spectral properties of these polymers, with particular reference to p-doping induced charged states. These findings provide new insights into the factors requiring attention during structure tailoring of donor – acceptor assemblies for organic optoelectronic applications.

Introduction

In a quest to prepare tailored π-conjugated polymer systems different molecular architecture strategies have been proposed and prospected. Progressing from homopolymer structures, hitherto pursuits have identified the donor – acceptor molecular architecture concept as the most versatile in affording polymer structures of desired electronic and spectral properties.[1] Considering provisions for material processing ability, the polymer solubility issue is often at stake and one of the ways found to effectively address it is to graft the monomers with bulky alkyl groups, whose solvent compatibility (solvation ability) affords solubility of the macromolecular chain to which they are attached. Their presence is not inert though and the impact of these side groups on both electronic and structural properties of π-conjugated systems has been reported[2–4]. Other types of substituents bearing certain functional groups can be incorporated to modify the physical properties such as energy levels, absorption, emission and morphology[5,6]. HOMO and LUMO orbital energy levels, and hence energy gap, can be tuned by different inductive or resonance effects. Electron withdrawing groups lower orbital energy levels while electron donating groups raise these. First group of substituents include aldehyde[7], malononitrile[8], alkylsulfonyl[9] and fluoroalkyl[10] groups. The latest include alkoxyl[11], alkyloamino and acetate groups.

Side groups often lead to improved self-ordering yielding enhanced charge mobility[12], but in other cases they can impair the electric conductivity due to steric hindrance. Special kind of interaction caused by side groups is observed in the case of poli(3,4-ethylenedioksythiophene) (PEDOT). Strong interaction between O and S atoms of neighbouring EDOT units leads to rigidification of polymer chains, effectively extending the effective conjugation length[13]. This effect affords PEDOT its exceptional electrochemical and optical properties, which contribute to numerous commercial applications of this polymer[14]. Sulphur derivative of EDOT- 3,4-ethylenedithio-

[a] Silesian University of Technology, Faculty of Chemistry, Department of Physical Chemistry and Technology of Polymers,
ul. Marcina Strzody 9, 44-100 Gliwice, Poland.
email: wojciech.domagala@polsl.pl; tel.: +48 322371305
[b] University of Strathclyde, Department of Pure and Applied Chemistry,
295 Cathedral Street, Glasgow G1 1XL, United Kingdom

† Electronic Supplementary Information (ESI) available: NMR spectra of synthesised compounds and auxiliary EPR data. See DOI: 10.1039/x0xx00000x

View Article Online
DOI: 10.1039/C5RA06993A

thiophene (EDTT) presents similar redox properties to EDOT[15], however polymer performance differs considerably due to weaker homonuclear interactions between sulphur atoms[13].

Polymers with donor-acceptor (D-A) structure have been studied extensively over the last decade, affording numerous targets with unique properties. This group of π-conjugated organic materials comprise electron-rich and electron-deficient units[16]. Some D-A polymers exhibited remarkable properties such as broad and strong absorption, narrow band gap, fast and reversible colour switching, high conductivity and high stability during oxidative and reductive doping processes [17–20]. These traits led them to find application in modern electronics like photovoltaics[21–23] organic field effect transistors[24] and electrochromics[18,25–27].

The benzothiadiazole (BT) molecule is one of the richest electron acceptor units used to tailor the position of LUMO energy level in D-A type polymers[28]. The electron-deficient BT unit has been attached to electron rich molecules such as thiophene derivatives, resulting in materials with interesting optical and electrochemical properties[29–33]. Numerous conjugated polymers with BT unit have been synthesized and characterized, with many demonstrating superior electrochemical and optical properties, for instance low HOMO-LUMO gap values, high conductivity, low oxidation potential, high optical contrast, fast switching time and intramolecular charge transfer (ICT) between the electron rich and deficient units [23,34–37].

In this paper, five structural monomers of donor-acceptor-donor class (DAD), featuring thiophene and its derivatives coupled to benzothiadiazole group, and their respective polymers have been investigated. Two different structural modification vectors have been pursued. One involves substitution of the thiophene groups with alkyl chain of different length, while the other furnishes the β positions of the thiophene groups with bridged 1,2-chalcogenoethylene units. The first structural variation targets the intermolecular interactions between polymer chains including packing, self-organisation and inter-chain charge transport. The second variation impacts the electronic properties of the π-conjugated bond, accounting for the energies of frontier molecular orbitals as well as intermediate states developing upon redox processes of these molecules and their polymers.

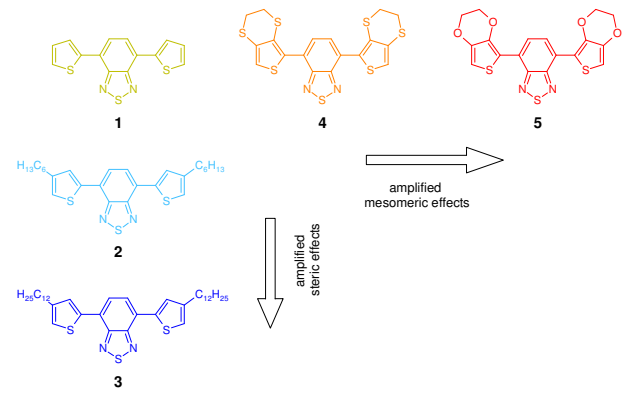

Chart 1 Repeating units of investigated polymers.

Polymers have been prepared electrochemically and studied using electrochemical and spectroelectrochemical methods affording *in situ* insight into the phenomena taking place during potential driven non-stoichiometric changes of the oxidation state of these macromolecules. Obtained results permit systematic structure-property relationships to be traced out and elucidated, showing the impact of different chemical moieties on the apparent electronic and optical properties of these materials which determine and translate to their material characteristics.

Experimental

Materials and Synthesis

The structures of investigated monomers are shown in Chart 1. 4,7-bis(thiophen-2-yl)-2,1,3-benzothiadiazole **1** (purity >98.0%(HPLC)(N)) was procured from TCI Europe, and following successful NMR check-up, used as received. Compounds 2-5 were synthesized according to the pathway illustrated in Scheme 1.

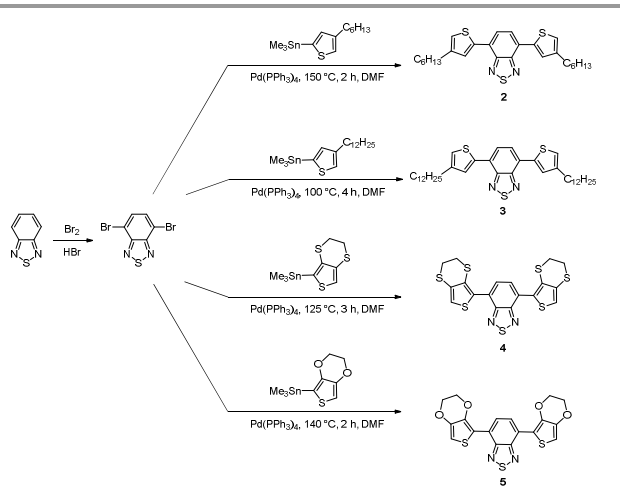

Scheme 1 The synthesis of compounds **2** through **5**.

Benzothiadiazole was dibrominated using HBr and Br_2. 3,4-ethylenedioxythiophene (EDOT), 3,4-ethylenedithiothiophene (EDTT), 3-hexylthiophene and 3-dodecylthiophene were stannylated *via* lithiation followed by the addition of Me_3SnCl at -78°C and used without further purification. Tetrakis(triphenylphosphine)palladium(0) ($Pd(PPh_3)_4$) was prepared prior to use and stored under nitrogen. Unless otherwise stated, all other reagents were sourced commercially and used without further purification. Dry solvents were obtained from a solvent purification system (SPS 400 from Innovative Technologies) using alumina as the drying agent.

^1H and ^{13}C NMR spectra were recorded on a Bruker Avance DPX400 instrument at 400.13 and 100.6 MHz or on a Bruker DRX 500 instrument at 500.13 and 125.76 MHz. Chemical shifts are given in ppm. Elemental analyses were obtained on a Perkin-Elmer 2400 analyser. MS LDI-TOF spectra were run on a

View Article Online
DOI: 10.1039/C5RA06993A

Shimadzu Axima-CFR spectrometer (mass range 1–150 000 Da). Thermogravimetric analysis (TGA) was performed using a Perkin-Elmer Thermogravimetric Analyzer TGA7 under a constant flow of helium. Melting points were taken using a Stuart Scientific instrument SMP1.

Compounds (**2**-**5**) were obtained in good yield (75, 62, 52 and 34% respectively) *via* microwave assisted Stille cross coupling in dimethylformamide using ($Pd(PPh_3)_4$) as the catalyst. The data for compounds **2**, **3** and **5** was consistent with that previously reported[38–40] and the data for 4,7-bis[2′-(3,4-ethylenedithiothiophene)]-2,1,3-benzothiadiazole **4** is as follows: ^{1}H NMR (400 MHz, $CDCl_3$): 7.88 (s, 2H, Ar-H), 7.23 (s, 2H, Ar-H), 3.33–3.30 (m, 4H, CH_2), 3.23–3.19 (m, 4H, CH_2) ppm. ^{13}C NMR (125 MHz, $CDCl_3$) δ = 153.49, 131.04, 129.44, 126.65, 125.91, 120.23, 98.05, 28.80, 28.08 ppm. All ^{1}HNMR spectra can be found in Figure S1 of ESI. MALDI TOF MS: m/z calculated for $C_{18}H_{12}N_2S_7$ $[M]^+$: 479.90 m/z; found: 479.83 m/z. Anal. calculated for $C_{18}H_{12}N_2S_7$: C, 44.97; H, 2.52; N, 5.83; found: C, 44.97; H, 2.50; N, 5.87%. TGA: 5% loss of the mass at 321°C. Melting point = 262-264°C.

Electrochemistry

Electrochemical measurements were performed in a classic three electrodes assembly with Pt disc electrode as the working electrode, Pt spiral as the counter electrode and Ag wire as pseudo-reference electrode. All experiments were conducted in dichloromethane (DCM) (Sigma-Aldrich, Chromasolv for HPLC), acetonitrile (ACN) (Sigma-Aldrich, Chromasolv for HPLC), tetrahydrofuran (THF) (Alfa Aesar, 99,5% extra dry) or in DCM/ACN solvent mixture. 0.1 M tetrabutylammonium hexafluorophosphate (Bu_4NPF_6) (TCI 98%) was used as the supporting electrolyte. All solutions were deaerated for 15 minutes before measurements with argon gas. All measurements are referenced to formal potential of the ferrocene redox couple. Electrochemical measurements were done on CH Instruments 620 potentiostat.

Spectroelectrochemistry

Polymer films were deposited electrochemically directly on ITO electrodes. After synthesis, polymer layers were rinsed with fresh solvent, immersed in 0.1M Bu_4NPF_6/ACN electrolyte and electrochemically dedoped. Optical spectroelectrochemical cell adapted for simultaneous EPR, UV–vis–NIR and electrochemical measurement was used. The spectroelectrochemical cell comprises two cylindrical quartz tubes holding the supporting electrolyte and intermediate EPR signal-free quartz flat capillary section of 0.5mm thickness. There, 0.3 mm ITO electrodes (PGO Optics, Germany) covered with polymer film were positioned giving thin layer electrolyte solution electrical contact which afforded acceptable EPR spectrometer tuning parameters. Teflon coated Ag pseudo-reference electrode was positioned next to the ITO electrode in the flat capillary part. Pt spiral counter electrode was assemble in the tube below the flat capillary section. Argon bubbling of electrolyte solution was kept uninterrupted through the top tube with the electrolyte effectively blanketing out the electrolyte solution from contact with air during spectroelectrochemical measurement.

EPR measurements were carried out using JEOL JES FA-200, X-band CW-EPR spectrometer, operating at 100 kHz field modulation, while UV–vis–NIR measurements were carried out using Ocean Optics QE65000 and NirQuest512 diode-array spectrometers, coupled with DH-BAL2000 light source. EPR spectrometer were equipped with ES-MCX3B transmission cavity operating in TE_{012} mode. Light for UV–Vis–NIR measurement was supplied and collected by optical fibres. Potential was applied by Autolab PGSTAT100N potentiostat. EPR and UV-Vis-NIR spectra have been collected *in situ* at stepwise applied potentials in the anodic range during p-doping and dedoping. This procedure was changed in the cathodic range due to different characteristic of reduction processes and different electrochemical stability of n-doped polymers.

Spectroelectrochemical measurements of p-doping and dedoping states of polymers were made after reaching doping equilibrium at each applied potential, which usually required several seconds. In this manner, time independent EPR or UV-Vis-NIR spectra were recorded. EPR spectra were measured twice at every potential for two different modulation widths, to ensure the best conditions to estimate g-value, relative spin concentration and linewidth (ΔB_{pp}). The relative concentrations of paramagnetic species was determined by double integration of the first-derivative EPR spectra with baseline correction. The g-factor of the radicals was determined using a JEOL internal standard – the $^{55}Mn^{2+}$ radical, whose 3rd hyperfine line has a g-factor of 2.03323. ΔB_{pp} of EPR signal was estimated from spectra recorded with modulation amplitude equal or lower than 0.25 of the narrowest signal linewidth. High signal to noise ratio is required for measurements aimed at estimation of concentrations of paramagnetic species. This can be achieved by setting high modulation amplitude. To estimate the best signal to noise ratio the same modulation amplitude was used, being chosen as 1.5 of the narrowest ΔB_{pp}. This value was in the linear range of dependence of signal intensity estimated from double integration of EPR signal and modulation amplitude. Second EPR spectra was recorded at modulation amplitude chosen as 0.25 of the narrowest ΔB_{pp}. At this parameter only negligible deformation of EPR line shape is observed and hence the linewidth of EPR signal can be estimated[41].

The procedure of spectroelectrochemical measurement during cathodic (n-) doping and dedoping was different. The reduction potential was chosen as the reduction peak potential of the polymer CV. Contrary to p-doping, the n-doping equilibrium required much longer times to achieve, usually several minutes. Spectra were recorded after attaining the electrochemical equilibrium. EPR spectra were recorded only at modulation amplitude chosen to be 0.25 multiple or lower of the ΔB_{pp} of the narrowest polymer EPR signal. This was done to enhance the signal to noise ratio of cathodic range EPR spectra, compared to anodic potential range ones.

View Article Online
DOI: 10.1039/C5RA06993A

Results and discussion

Electrochemistry

Electrochemistry of investigated monomers and polymers was surveyed by cyclic voltammetry in DCM, ACN, THF or mixed DCM/ACN electrolyte environments. Different solvents were chosen due to significant differences in the solubility of studied compounds (both monomers and polymers alike) and different electrochemical stability windows of solvents in the anodic and cathodic ranges.

Cyclic voltammetry curves recorded in DCM exhibit quasi-reversible redox pair in cathodic range and irreversible peak in the anodic range (Figure 1). The cathodic range redox pair is attributed to the semi-reversible reduction of the BT unit. BT is known to be a strong electron acceptor. THF was chosen to widen the cathodic potential range, and cyclic voltammetry performed in this solvent displays two, well separated reduction peaks, first reversible and second irreversible (Figure 2). Discrete electrochemical data is summarized in Table 1. The difference of oxidation potential values of the monomers comes from different side group effects. Monomer **5** has the lowest oxidation potential compared with other monomers. It is consistent with earlier reports about diminished ionisation potential of EDOT compared to other thiophene units.

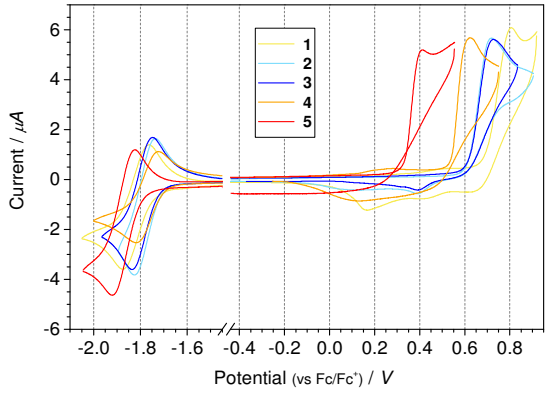

Figure 1 Cyclic voltammetry of compounds **1**-**5** in cathodic and anodic range; concentration $1 \cdot 10^{-3}$ M; 0.1 M Bu_4NPF_6/DCM; scan rate 0.1 V·s^{-1}.

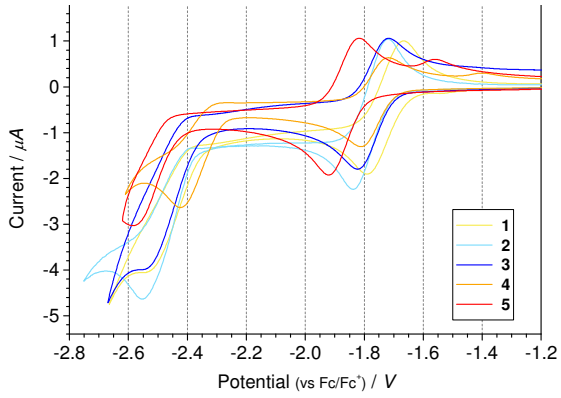

Figure 2 Cyclic voltammetry of compounds **1**-**5** in extended cathodic range; $1 \cdot 10^{-3}$ M solutions in 0.1 M Bu_4NPF_6/THF; scan rate 0.1 V·s^{-1}.

Table 1 Redox and electronic properties of monomers and polymers. IP – ionization potential estimated from equation $\mathrm{IP} = 5.1 + E^{ox}_{onset}$; EA - electron affinity estimated from equation $\mathrm{EA} = 5.1 + E^{red}_{onset}$; ΔE^{el}_g - electrochemical energy gap estimated from equation $\Delta E^{el}_g = \mathrm{IP} - \mathrm{EA}$; ΔE^{op}_g – optical energy gap estimated from equation $\Delta E^{op}_g = 1240/\lambda_{onset}$ where λ_{onset} is the onset of absorption edge.

compound	E^{ox}_{onset} [V]	E^{red}_{onset} [V]	IP [eV]	EA [eV]	ΔE^{el}_g [eV]	ΔE^{op}_g [eV]
1	0.69	-1.74	5.8	3.4	2.4	2.44
2	0.62	-1.71	5.7	3.4	2.3	2.36
3	0.62	-1.71	5.7	3.4	2.3	2.36
4	0.53	-1.70	5.6	3.4	2.2	2.39
5	0.33	-1.77	5.4	3.3	2.1	2.25
p1	0.34	-1.52	5.4	3.6	1.8	1.61
p2	0.30	-1.57	5.4	3.5	1.9	1.61
p3	0.36	-1.60	5.5	3.5	2.0	1.57
p4	0.30	-1.4	5.4	3.8	1.7	1.75
p5	-0.68	-1.66	4.4	3.4	1.0	1.26

All monomers are well soluble in DCM and THF. However, the electrochemical polymerization of **2** and **3** in DCM leads to formation of soluble products. ACN is a poor solvent for compounds with long alkyl substituents, For this reason, electropolymerisation of compounds **2** and **3** was studied in a mixed DCM/ACN solvent system. Proper ratio of these solvents afford 1mM solubility of compounds **2** and **3** with simultaneous insolubility of products formed as a result of their electrooxidation and subsequent electropolymerisation.

Repetitive anodic cyclic voltammetry of compounds **1** through **5** is presented in Figure 3. In all cases, from the first oxidation half-cycle onwards, mounting current response, both during oxidation and reduction half-cycles is observed. Simultaneously, an electrochromic film deposit appears at the working electrode. Redox peaks at lower potentials appear as a results of formation of compounds with extended conjugation length at the electrode surface. These results indicate that electrochemical polymerization following well-known electrodeposition mechanism of conjugated polymers[42] is taking place here.

Owing to at least partial solubility of electrodeposited polymer films in DCM, their cyclic voltammetry was performed in ACN in which they are completely insoluble. The electrochemical responses of thin insoluble films of polymers **p1** through **p5** are given in Figure 4. The characteristics of voltammetric curves depend on structure of thiophene derivative units, but the results indicate that all polymers can be reversibly cycled. Considering the influence of alkyl substituents on the redox properties, the current ratio between n-doping and p-doping was taken into account. CV of **p1** displays sharp and reversible reduction. The current ratio between n- and p-doping clearly decrease in order **p1** > **p2** > **p3**. The increased length of alkyl substituents deteriorate the n-doping ability of polymer films. This can be explained by the alkyl chain spacing effect moving polymer chains apart with increasing volume of alkyl groups. This impairs the inter-chain electron transfer and hence reduces the hopping mobility of charge carriers between electron acceptor moieties.

View Article Online
DOI: 10.1039/C5RA06993A

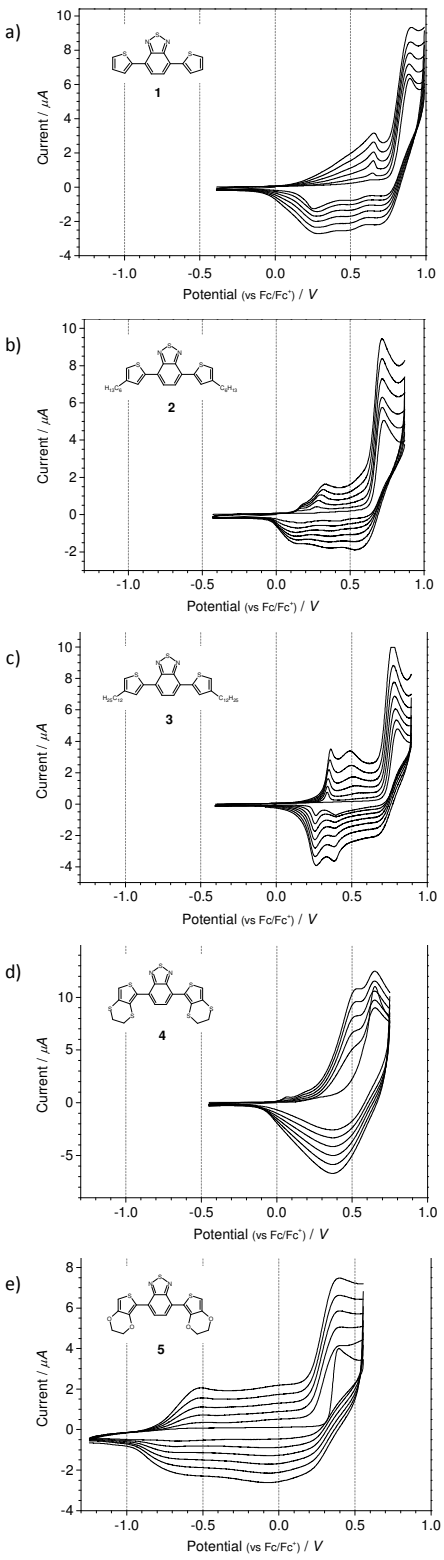

Figure 3 Cyclic Voltammetry of anodic electrochemical polymerization of investigated monomers. Monomers **1**, **4** and **5** dissolved in DCM; **2** in DCM:ACN mixture (1:1 v/v); **3** in DCM:CAN mixture (1:3 v/v) with 0.1 M Bu_4NPF_6 as supporting electrolyte. Scan rate 0.1 $V \cdot s^{-1}$.

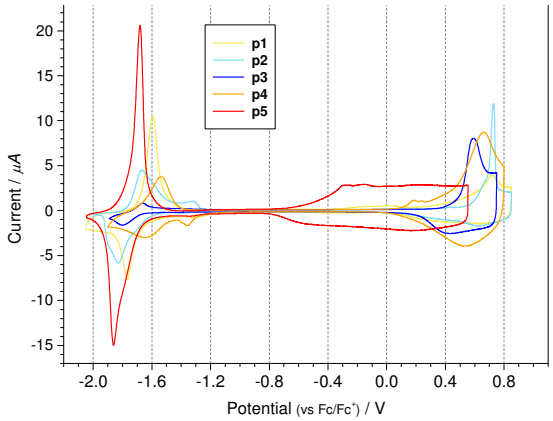

Figure 4 Cyclic Voltammetry of polymer films recorded in 0.1 M Bu_4NPF_6 / ACN . Scan rate 0.1 Vs^{-1}.

Oxidation onset of **p5** is strongly shifted to lower potential values compared to **p1** and its alkyl derivatives. This characteristic effect of EDOT derivative polymers is primarily attributed to intramolecular chalcogen–chalcogen interactions. Strong oxygen - sulphur intramolecular interaction between neighbouring EDOT units rigidify the polymer chain and increase the effective conjugation length[13]. Similar effect is much weaker in **p4** due to absence of dipolar sulphur - sulphur interactions.

UV-Vis spectroscopy

Absorption spectra of monomers **1-5** recorded in DCM solution are shown in Figure 5, while the absorption spectra of electrochemically undoped polymers **p1** through **p5**, electrosynthesised at ITO electrode, are presented in Figure 6. The absorption spectra of all monomers are similar in shape featuring at least three peaks. The lowest energy peak can be assigned to ICT[37] between the donor and acceptor units. For polymers, this peak is red-shifted and concealed in the low energy tail of the dominant absorption band. ICT band is commonly observed in the D-A type conjugated molecules, both low molecular weight materials and polymers containing BT in their structure with different thiophene derivative units[43–49]. Characteristic properties of this type of molecules such as low energy gap and strong broad absorbance are important in photovoltaic and electrochromic applications[48,49]. Higher energy peaks correspond to different more energetic π-π* transitions.

The spectra of monomers **2** and **3** are bathochromically shifted compared to **1** as a results of positive inductive (electron donating) effect of alkyl substituents. The comparison of corresponding electrochemically deposited polymers is more complex. Additional factors such as intermolecular interactions in the polymer film, charge trapping, different molecular weight and hence different effective conjugation length can influence the absorption spectra. Spectra of **p2** and **p3** reveal maxima at shorter wavelengths than **p1** spectrum. This result indicates greater contribution of steric factors in polymers than in monomers. Inductive effect

View Article Online
DOI: 10.1039/C5RA06993A

of alkyl substituents appears unable to compensate for these in polymers.

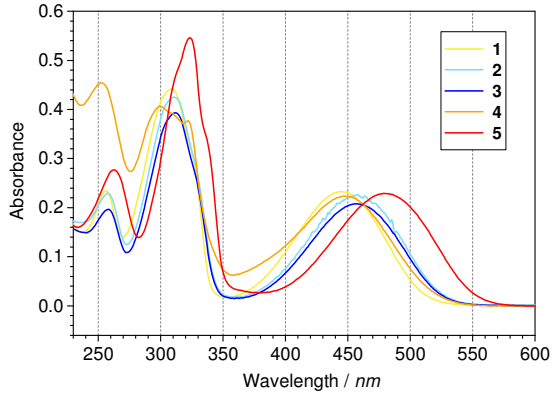

Figure 5 UV-Vis spectra of $1 \cdot 10^{-3}$ M solutions of compounds **1**-**5** in DCM.

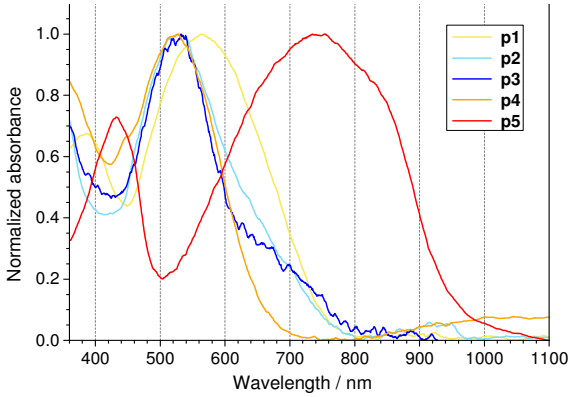

Figure 6 Normalized UV-Vis spectra of undoped, electrochemically deposited **p1** through **p5** polymer films at ITO electrode.

Comparison of spectra of **1**, **4** and **5** and their corresponding polymers was carried out to determine of effects of heteroatom based bridges. The absorption peaks of compound **4** are only slightly bathochromically shifted compared to spectrum of **1**, while **p4** is hypsochromically shifted compared to **p1**. Both spectra of monomer **5** and **p5** present bathochromic shift. However the shift in the case of monomer **5** is 0.2 eV while for **p5** it increases up to 0.56 eV. These results indicate high influence of mesomeric effect in the lower molecular weight compounds and the significant increase of influence of steric effects in the polymer films. Stiffening of **p5** structure by oxygen-sulphur interaction leads to increase of effective conjugation length while twisting of the structure of **p4** leads to reduction of effective conjugation length that impacts absorption spectra accordingly[50]. These results confirm the cooperative inductive and mesomeric effects of substituents on properties of ambipolar molecules. However these effects are significantly different for low molecular weight and high molecular weight compounds. The impact of steric effects is more pronounced for polymers.

Electronic properties

Electronic properties of monomers and polymers have been determined from cyclic voltammetry and UV-Vis spectra. The results are collected in Table 1.

Monomer **1** has an IP value of 5.8 eV. The IP value of **5** is equal to 5.4 eV as a results of electron donating effect of 3,4-ethylenedioxy substituent and the rigidity effect described earlier. Similar, though much weaker effect, is observed for monomers **2**, **3** and **4** with intermediated IP value equal to 5.7 eV. All monomers present similar EA values, ranging from 3.3 eV up to 3.4 eV. ΔE_g^{el} and ΔE_g^{op} are similar in value, their difference does not exceed 0.2 V. In both cases, monomer **5** demonstrates the lowest values of these parameters.

For all polymers, the decrease of EA and increase of IP compared to monomers is observed. IP of **p1**, **p2**, **p3** and **p4** is lower than monomers approximately 5.4 eV. Compared to monomers only 0.3 eV shift is observed. Much greater difference is observed in the case of compound **5** which oxidative electrodeposition gives a polymeric product with EA of 4.4 eV. Once again this effect stems from strong heteroatom interactions in the polymer chain. Compared to pure PEDOT only slight change of the IP occurs. The conjugation between bisEDOT units formed as a results of electrochemical oxidation of monomers is not interrupted at BT units, afforded by p-benzoquinoidal type of structure at BT moiety. The influence of substitution on EA values is smaller, however. It is typical for compounds with BT acceptor unit, whose LUMO is localized mainly at the 1,2,5-thiadiazole moiety.[51]

Calculated ΔE_g^{op} values of monomers were found to be from 2.23 eV up to 2.44 eV. ΔE_g^{el} was estimated to be 2.3 eV for **2** and **3**, 2.2 for **4** and 2.1 for **5**. Greater differences between studied compounds were found in the case of polymers. The trend of ΔE_g^{el} and ΔE_g^{op} of polymers is similar to monomers. In the polymers case, narrowing of those values is observed. The narrowest energy gap characterize **p5** mainly as a results of change of HOMO level. The differences between ΔE_g^{el} and ΔE_g^{op} for polymers can be explained as an effect of additional electrochemical processes taking place at the working electrode, such as reorganization and charging of the polymer film structure and different overpotential components.

EPR/UV-Vis-NIR spectroelectrochemistry

The role of structure of the electron donor units on properties of D-A type of conjugated polymers were investigated by detailed triple EPR-UV-Vis-NIR spectroelectro-chemistry. EPR and UV-Vis-NIR spectra have been collected *in situ* at stepwise applied potentials according to procedure described in the experimental section.

p-Doping.

Starting from the potential at which polymers were in their neutral form the potential was gradually increased. Electrochemical p-doping was performed up to the stability

View Article Online
DOI: 10.1039/C5RA06993A

potential threshold of the polymer film, estimated from its repetitive CVs at incremented maximum anodic potentials.

Selected EPR spectra of **p2** electrodeposited at ITO electrode are shown in Figure 7, while spectra of other polymers shown in Figure S2 of ESI). Spectrum recorded at 0 V shows EPR signal of small intensity. Signal intensity begins to increase at potential slightly below E_{onset}^{ox}. This offset comes from a small ohmic drop, inherent to the potentiodynamic measurement of cyclic voltammetry, compared to potentiostatic mode employed for EPR spectroelectrochemical studies here. In the p-doping half-cycle the EPR lines change their intensity and linewidth for all five polymers studied. Increase of EPR line intensity at the beginning of the oxidation process is observed for all four polymers indicative of radical cation species being generated. The changes in shape and intensity of spectral lines taking place throughout the p-doping range, were analysed in detail.

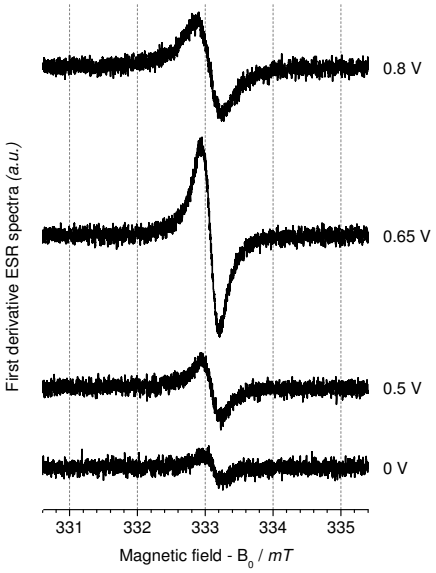

Figure 7 Selected EPR spectra of **p2** electrodeposited at ITO electrode, in 0.1M Bu4NPF6/ACN solution, recorded *in situ* at progressively incremented potentials applied to the film. For spectra of other polymers, see Figure S2 of ESI.

Taking advantage of the triple spectroelectrochemical technique employed, simultaneous UV-Vis-NIR spectra were recorded (Figure 8). UV-Vis-NIR spectra of polymers in their neutral state show clear dependence of the transition energy on the polymer structure. The spectra of all polymers start to change at the beginning of oxidation. New absorption bands appear in the lower energy range. The formation of these new transitions is associated with formation of polaron and bipolaron charge carriers in conjugated polymer backbone. In Figure 8 - subfigures f) through j), the difference spectra are also shown in order to better visualise the changes in absorption bands between pairs of consecutive spectra, helping to characterise redox processes taking place at different p-doping levels. By virtue of simultaneous acquisition, comparison of UV-Vis-NIR changes with data obtained from EPR spectral analysis was feasible.

First aspect taken into consideration is the influence of alkyl substituents on the course of p-doping process. E_{onset}^{ox} is similar for **p1** and its alkyl derivatives **p2** and **p3**. At the beginning of oxidation the relative concentration of spins increase sharply (Figure 9). Simultaneously, the formation of two broad absorption bands at approximately 800 nm and 1400 nm is observed. At higher p-doping levels, new band appears. The overlapping of different electron transitions and simultaneous increase of different peaks takes place in broad potential range. At high doping level, the changes of transition bands correlate with changes of relative spin concentration. The relative spin concentration increase up to 0.75 V (**p1**), 0.7 V (**p2**) and 0.58 V (**p3**). In these potential ranges, bands of different electron transitions increase. Going past these potentials, the band at 1200 nm increases most prominently in the UV-Vis-NIR spectra. Simultaneously the relative spin concentration begins to decrease signifying commencement of domination of spin paired species in the doped films.

The comparison of p-doping of polythiophene D-A type derivatives with common polythiophenes reveals some similarities[52]. The formation of spin bearing molecules with g-factor 2.0023 at the beginning of oxidation and two strong absorption bands indicate formation of polarons. At higher doping level the simultaneous appearance and increase of different overlapping absorption bands and increase of relative spin concentration indicate simultaneous formation of polarons and spinless species. The equilibrium between both type of charge species takes place across broad potential range. Their ratio changes with increasing potential as can be seen on the UV-Vis-NIR spectra. The g-value slightly shifts up to 2.0026 (**p1**) and 2.0025 (**p2** and **p3**) indicating change of the radical environment with increasing doping level. At high doping levels, only spinless species, featuring only one principal transition band are generated. These spinless species are explained by bipolaron, dicationic interchain π-dimers or σ-dimers model[42,52,53].

Analysing the electrochemical dedoping process, the hysteresis in number of spin bearing species is observed. This feature is also present on polymer CVs in the form of an offset of polymer film reduction currents into lower potentials. In the case of solid state electrochemistry of conjugated polymers, hysteresis is often observed and its explanation is still a matter of discussion. It is interpreted by different kinetic and thermodynamic effects[42]. Initial explanations include charge diffusion during charging and discharging or conformation changes. However thermodynamic explanation focus on formation of energetically more stable interchain σ-dimers with more negative formal redox potential than neutral polymer, spin pairing into π-dimers[54] or the stability of quinoid structure of bipolaron species[55].

View Article Online
DOI: 10.1039/C5RA06993A

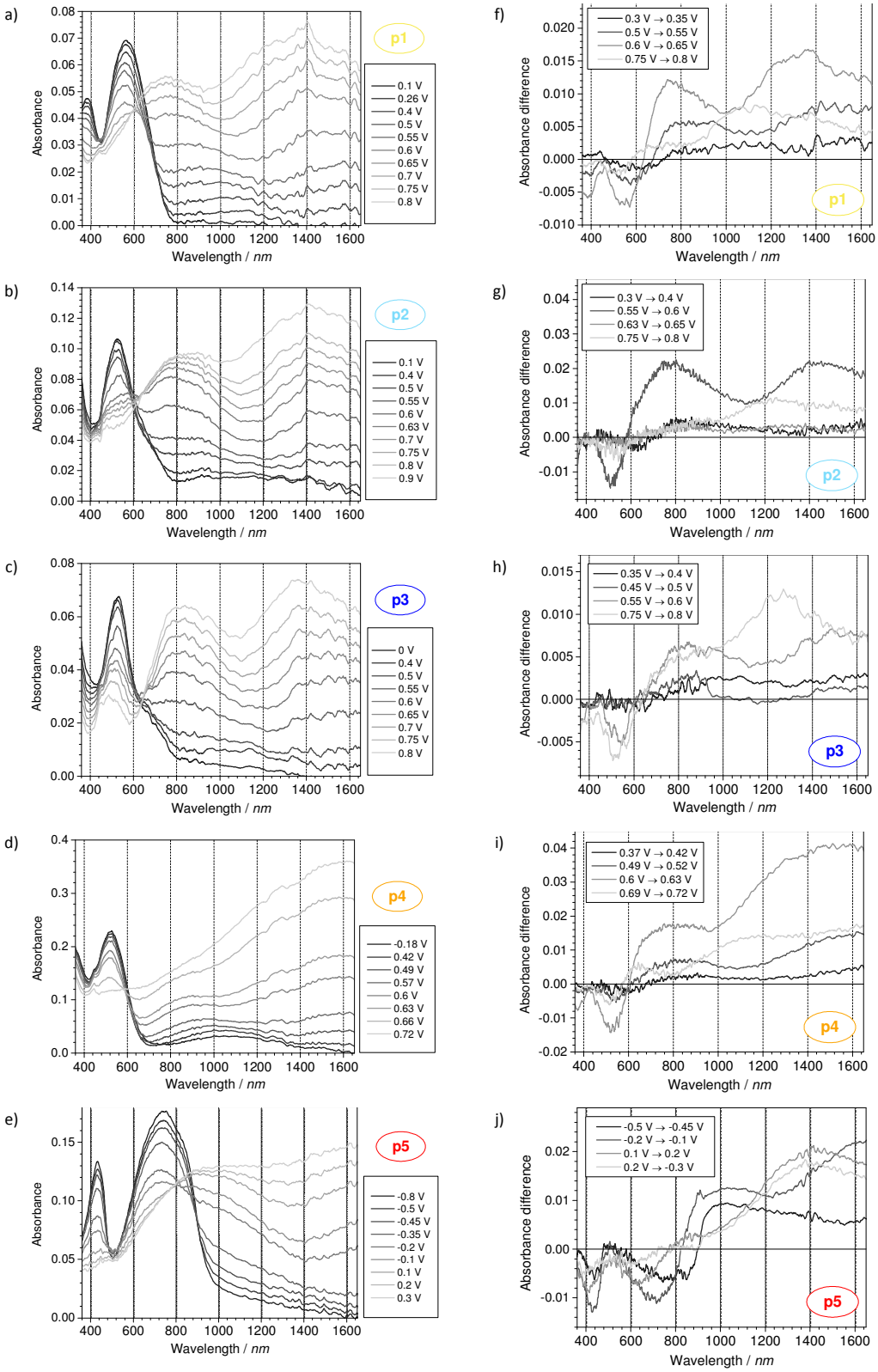

Figure 8 Selected UV-Vis-NIR spectra (left) and their difference spectra (right) of polymer films electrodeposited at ITO electrode, in 0.1M Bu_4NPF_6/ACN solution, recorded *in situ* at progressively incremented potentials applied to the film during electrochemical p-doping.

View Article Online
DOI: 10.1039/C5RA06993A

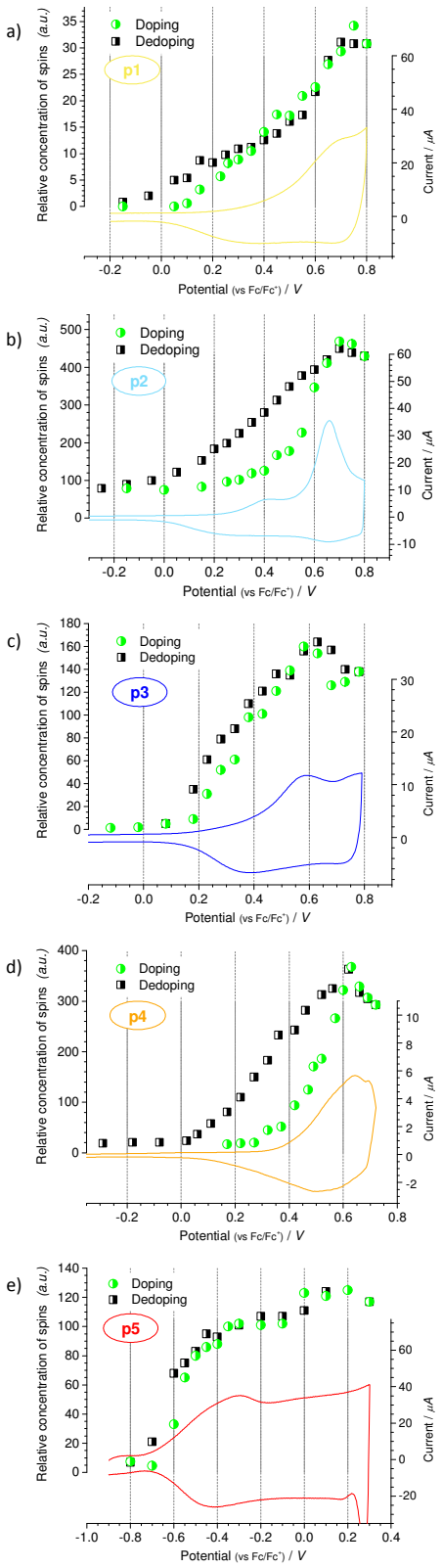

Figure 9 Relative concentration of spins in polymers **p1** through **p5**, as a function of applied potential during their p-doping and subsequent dedoping in 0.1M Bu_4NPF_6 / ACN. Overlaid CVs show the response of investigated polymer films at employed spectroelectrochemical conditions.

p-Doping and dedoping of **p4** also takes place with formation of polarons at the beginning of oxidation and spinless species at higher potentials. Characteristic polaron peaks are located at approximately 800 nm and 1500 nm, spinless species at approximately 1150 nm. EPR signal of generated **p4** radical is centred at g-value 2.0038 at low doping levels and 2.0042 at high doping level. These values are significantly higher compared to **p1** and free electron value g=2.0023. This indicates substantial contribution of the ethylenedithio- sulphur atoms orbitals to the radical cation orbital in oxidized **p4**.

Careful inspection of **p5** reveals more complex course of changes of concentration of paramagnetic species than those taking place in other studied polymers. At this point, we also compare obtained results with those, previously reported by our group for PEDOT doping[56]. The strong shift of E_{onset}^{ox} to lower potential values observed in PEDOT voltammetry (approximately -0.9 V)[56] is preserved in **p5** voltammetric characteristics (-0.68 V). The CV of **p5** and its concentration of spins is slightly shifted to more positive potentials than in the case of PEDOT. The trend at the beginning of doping is similar with increase of spin concentration up to -0.45 V. In this range, overlapping of the neutral polymer transitions and first strong polaron transition is observed on UV-Vis-NIR spectra. After passing this potential, overlap with subsequent transition bands can be seen. The relative spin density fluctuates and then slightly increase in contrast to PEDOT. The spin density of PEDOT after reaching -0.4 V decrease monotonously. This is also reflected in CV of both polymers. The CV current of **p5** past the first distinguishable peak at approximately -0.3 V slightly decreases and then increases, in contrast to CV of PEDOT where monotonous decrease is observed. This can be attributed to the superposition of several redox states characteristic in conjugated polymers of long chain length. The presence of several redox states can be linked to formation of different charge carriers in crystalline and amorphous polymer phases. Similar interpretation was proposed and studied in detail for electrochemically generated PEDOT[56].

In order to elucidate the character of spin bearing carriers in **p5** the changes of linewidth of EPR signal and g-factor were evaluated (Figure 10). Simultaneously with change of spin density, significant change of linewidth of EPR signal is observed. Analysing the g-factor potential dependency plot, three regions can be distinguished. In the initial range, up to -0.35 V, a constant g-factor value of 2.0026 is maintained. At higher potentials, g-factor increases slightly, pointing to increase of spin density at S, N or O heteroatoms. Simultaneously ΔB_{pp} begins to increase, indicating increased localization of the cation radicals. At higher doping level, sharp increase of g-factor up to 2.0031 and further ΔB_{pp} increase are seen. The g-factor values of oxidized **p5** are larger than in **p1** but lower than in **p4**. This indicates distinct contribution of oxygen orbitals of the ethylenedichalcogeno bridge to the radical cation orbital, although less prominent than that of sulphur.

View Article Online
DOI: 10.1039/C5RA06993A

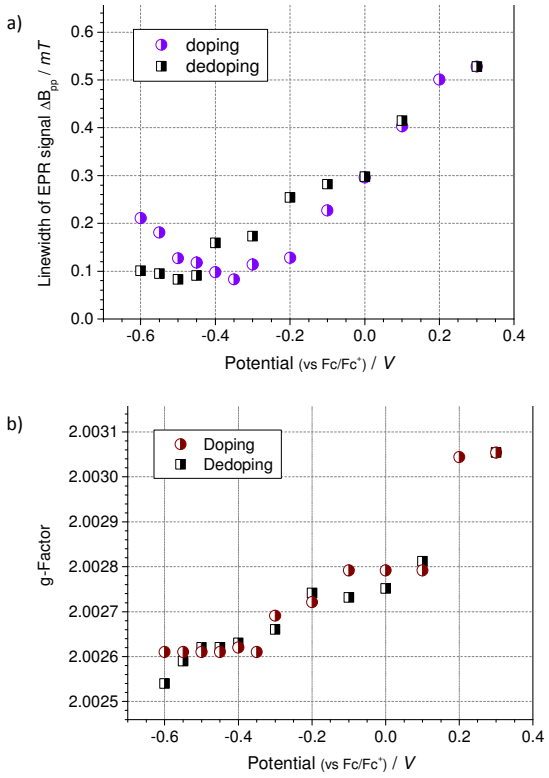

Figure 10 a) Linewidth (ΔB_{pp}), and b) g-factor of EPR signal of **p5** as a function of applied potential during its electrochemical p-doping and subsequent dedoping in 0.1M Bu_4NPF_6 / ACN. For potential dependencies of EPR signal linewidth of other polymers, see Figure S3 of ESI.

n-Doping.

EPR and UV-Vis-NIR spectra of studied polymers were also recorded during cathodic (n) doping and dedoping (Figure 11), spanning the potential range of their first reversible reduction CV peak. The character of reduction processes turns out different than during oxidation. Already at the beginning of reduction, the EPR signal appears in all studied polymers. Simultaneously UV-Vis-NIR spectra begins to change. New absorption bands appear in the low energy range. The energy of these new bands is different than corresponding absorption bands emerging during p-doping. For an applied reduction potential, the electrochemical equilibrium at which UV-Vis-NIR and EPR spectra do not change further is achieved after longer time, compared to p-doping regime. This time can reach several minutes and depends on the polymer and thickness of its film. In contrast to p-doping, UV-Vis-NIR spectra of n-doped species increase homogenously in the whole potential range related to the first reduction peak. No additional transitions are observed at higher doping levels. Simultaneously the appearance of radical anion is confirmed by the formation of potential responsive single isotropic Lorentz type EPR line (Figure 12). The change of both EPR and UV-Vis-NIR spectra are related to each other. This indicates that only one type of reduced spin-bearing species appears in the n-doped systems, and that these species are radical anions. It is indeed intriguing

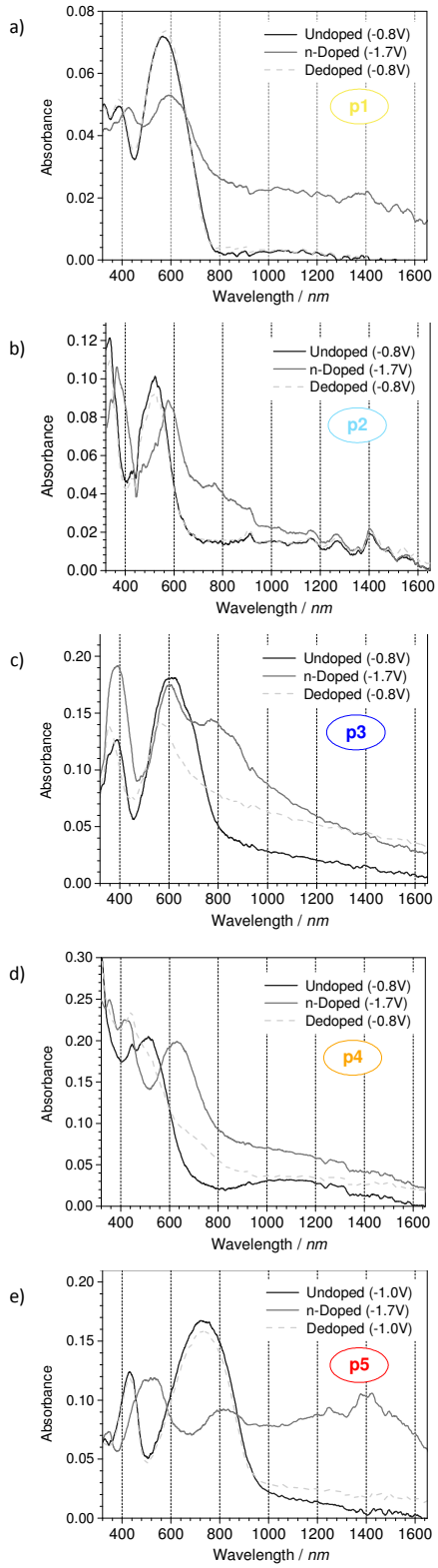

Figure 11 UV-Vis-NIR spectra of electrodeposited polymer films of **p1** through **p5** at ITO electrode in 0.1M Bu_4NPF_6/ACN solution, at three indicative states: undoped (before n-doping), n-doped, and after dedoping, revealing partial charge trapping.

View Article Online
DOI: 10.1039/C5RA06993A

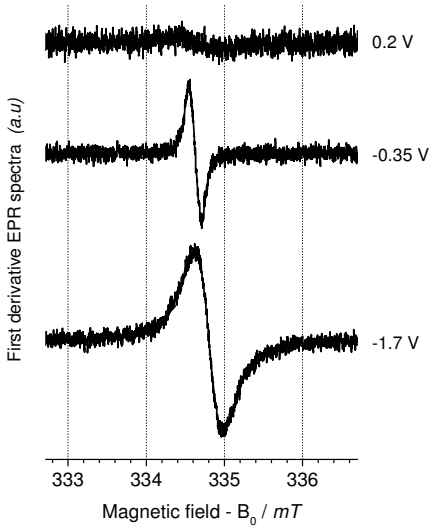

Figure 12 Selected EPR spectra of **p5** electrodeposited at ITO electrode, in 0.1M Bu_4NPF_6/ACN solution, recorded *in situ* at progressively incremented cathodic potentials applied to the film.

that no trace of spinless dianions is detected. This is probably related to discrete reduction steps of the monomers, whereby two clear reduction waves have been observed, ascribable to two consecutive reduction steps, first to radical anion, and the second one to dianion. The fact that only radical anions develop at the first reduction step of the polymer indicates that one would need to progress down the potential axis to the second redox step to observe the reduction of the polymer radical anions, and that these two processes do not overlap each other.

The g-factor of radical anions is similar for all studied polymers which are 2.0040 – **p1** and **p2**, 2.0041 – **p3**, 2.0042 **p4** and **p5**. The strong shift of g-factor value comparing to free radical confirm high spin distribution at heteroatoms. Sulphur and oxygen atoms substituted to the main polymer chain in **p5** and **p4** elevate the g-factor. This indicate delocalization of radical anions mainly at the BT unit but also which carries nitrogen and third period sulphur atom enhancing spin-orbit coupling spin interactions which elevate the g-factor of spins localised at it. This, further implies that benzothiadiazole based radical anions are much more localised that their radical cation counterparts and, due to their stepwise redox behaviour, do not interact with each other since no pairing of them is observed upon their electrochemical inception. The observation of slow electrochemical equilibration of the n-doped polymer state at a given cathodic potential seems to further support this inference, since non-interacting radical anions behave like localised charge carriers impairing can be traced to impaired conductivity of n-doped polymer film. This situation is also reflected in n-doping charge trapping observed as UV-Vis-NIR bands and residual EPR signal, in a polymer film, re-oxidised back to electroneutral state. with the effect becoming more pronounced with increased thickness of polymer films.

Comparison of relative spin concentrations in **p5** in p- and n doping range was also made. This polymer film has been chosen owing to its best electrochemical stability during n-doping. **P5** film was oxidized and then reduced in the same EPR experimental setup and conditions. The ratio of double integral of EPR signal of radical anion in the first reduced state and the radical cation EPR signal of maximum intensity, was found to exceed 6. Assuming all BT unit undergo reduction, and, to the first approximation, the radical cation and radical anion EPR relaxation times are taken as equal, the number of spins per unit in p-doping can be estimated. Such comparison yields the maximum spin concentration as 0.16 spins per monomer unit or 0.11 per bis-EDOT repeating unit. This value amounts to half the maximum spin concentration of 0.12 spins per EDOT unit obtained from quantitative measurement of PEDOT[56], neatly pointing to comparable spin pairing propensity of EDOT based polymers, despite the presence of electron-accepting in the polymer architecture.

Cyclic voltammetry together with spectroelectrochemical studies demonstrate fundamental differences between p- and n-doping regimes of studied bis(thiophene)-benzothiadiazole motif polymers. While the oxidation lead to simultaneous formation of different positive charge carriers - spin-bearing polaron and spinless species, reduction leads to discrete formation of only one type of charger carrier - negative polaron, within the range of potentials accessible in this study. These differences translate to broad and diffused voltammetric oxidation signatures and sharp, exhaustive electrolysis like reduction peaks. Comparing these results with a report presenting irreversible CV of a few BT units linked together in series [57] it stands clear that not only the position of the LUMO level, but also proper balance between donor and acceptor units, as well as intra and inter-macromolecular architecture of the polymer are the determining factors of reversible n-doping ability and electrochemical stability of π-conjugated ambipolar systems.

Conclusions

The influence of different thiophene derivative donor units on benzotiadiazole acceptor class of conjugated architectures was studied from monomer to polymer. Structure-property interactions shaping the electronic properties of these donor-acceptor conjugated materials were elaborated. Thorough, comprehensive and conclusive insight into how different structural elements determine these properties was made by focussing on changing the local environment of the benzothiadiazole unit and rationalising the properties of such aggregates. Bringing together a suite of premier electro-optic techniques, triple EPR-UV-Vis-NIR spectroelectrochemistry in particular, an *in situ* concerted study of both p- and n- doping phenomena was carried out, demonstrating how different chemical factors play a role in the development and interactions of charge carriers in each of the two regimes, and how these interactions translate to the apparent physicochemical properties of the π-conjugated system at different charged states. Inductive, resonance and steric

View Article Online
DOI: 10.1039/C5RA06993A

effects were found to significantly impact the intra and intermolecular interactions in the investigated donor-acceptor polymers. The proper balance of different features of donor - acceptor π-conjugated structure, such as HOMO and LUMO level, matching of donor and acceptor units, arrangement and rigidity of polymer structure all proved important factors impacting the stability of both p and n-doped states.

Comparison of p- and n-doping processes was made in order to highlight differences between both types of doping. Different pathways leading to p- and n- doped equilibrium states were identified and rationalised. Different types of charge carriers were also found to prevail in the doped states, with closely interacting spin bearing and spinless cationic species supporting the p-doped state, while n-doped state was found to exclusively comprise loosely interacting radical anion species. Furthermore, performing in-situ p- and n- doping studies on the very same polymer sample, enabled us to draw qualitative comparative conclusions regarding the efficiency of generation of different kinds of charge carriers, providing new and important information about these two doping regimes. These results point to disparate doping mechanisms and resultant properties of p- and n- type doped states of the thiophene-benzothiadiazole donor-acceptor polymer class, offering clues to molecular design strategies of this ubiquitous ambipolar architecture of contemporary organic electronics.

Acknowledgements

This work was financed by Polish National Science Centre grant no. 2011/03/D/ST5/06042.

References

1 P. Bujak, I. Kulszewicz-Bajer, M. Zagorska, V. Maurel, I. Wielgus and A. Pron, *Chem. Soc. Rev.*, 2013, **42**, 8895.
2 L. Biniek, S. Fall, C. L. Chochos, D. V Anokhin, D. A. Ivanov, N. Leclerc, P. Ĺeŵeque and T. Heiser, *Macromolecules*, 2010, **43**, 9779–9786.
3 B. Wang, J. Zhang, H. L. Tam, B. Wu, W. Zhang, M. S. Chan, F. Pan, G. Yu, F. Zhu and M. S. Wong, *Polym. Chem.*, 2014, **5**, 836–843.
4 X.-Y. Wang, F.-D. Zhuang, X. Zhou, D.-C. Yang, J.-Y. Wang and J. Pei, *J. Mater. Chem. C*, 2014, **2**, 8152–8161.
5 Y. H. Wijsboom, Y. Sheynin, A. Patra, N. Zamoshchik, R. Vardimon, G. Leitus and M. Bendikov, *J. Mater. Chem.*, 2011, **21**, 1368–1372.
6 P. Data, M. Lapkowski, R. Motyka and J. Suwinski, *Electrochim. Acta*, 2013, **87**, 438–449.
7 Z. Gu, L. Deng, H. Luo, X. Guo, H. Li, Z. Cao, X. Liu, X. Li, H. Huang, Y. Tan, Y. Pei and S. Tan, *J. Polym. Sci. Part A Polym. Chem.*, 2012, **50**, 3848–3858.
8 H. Xie, K. Zhang, C. Duan, S. Liu, F. Huang and Y. Cao, *Polymer (Guildf).*, 2012, **53**, 5675–5683.
9 J. A. Schneider, A. Dadvand, W. Wen and D. F. Perepichka, *Macromolecules*, 2013, **46**, 9231–9239.
10 L. Yang, J. Tumbleston, H. Zhou, H. Ade and W. You, *Energy Environ. Sci.*, 2012, 6, 316–326.
11 P. Lévêque, L. Biniek, S. Fall, C. L. Chocos, N. Leclerc and T. Heiser, in *Energy Procedia*, 2011, vol. 31, pp. 38–45.
12 J. Mei and Z. Bao, *Chem. Mater.*, 2014, **26**, 604–615.
13 H. J. Spencer, P. J. Skabara, M. Giles, I. McCulloch, S. J. Coles and M. B. Hursthouse, *J. Mater. Chem.*, 2005, **15**, 4783.
14 J. Roncali, P. Blanchard and P. Frere, *J. Mater. Chem.*, 2005, 15, 1589.
15 W. Domagala, D. Palutkiewicz, D. Cortizo-Lacalle, A. L. Kanibolotsky and P. J. Skabara, *Opt. Mater. (Amst).*, 2011, **33**, 1405–1409.
16 J. Chen and Y. Cao, *Acc. Chem. Res.*, 2009, **42**, 1709–1718.
17 Z. Zhang and J. Wang, *J. Mater. Chem.*, 2012, **22**, 4178.
18 P. M. Beaujuge, S. Ellinger and J. R. Reynolds, *Adv. Mater.*, 2008, **20**, 2772–2776.
19 M. Gora, W. Krzywiec, J. Mieczkowski, E. C. Rodrigues Maia, G. Louarn, M. Zagorska and A. Pron, *Electrochim. Acta*, 2014, **144**, 211–220.
20 S. Soylemez, S. O. Hacioglu, S. D. Uzun and L. Toppare, *J. Electrochem. Soc.*, 2014, **162**, H6–H14.
21 E. Poverenov, N. Zamoshchik, A. Patra, Y. Ridelman and M. Bendikov, *J. Am. Chem. Soc.*, 2014, **136**, 5138–5149.
22 Y. H. Chen, L. Y. Lin, C. W. Lu, F. Lin, Z. Y. Huang, H. W. Lin, P. H. Wang, Y. H. Liu, K. T. Wong, J. Wen, D. J. Miller and S. B. Darling, *J. Am. Chem. Soc.*, 2012, **134**, 13616–13623.
23 M. L. Keshtov, D. V Marochkin, V. S. Kochurov, A. R. Khokhlov, E. N. Koukaras and G. D. Sharma, *J. Mater. Chem. A*, 2014, **2**, 155–171.
24 Y. Deng, Y. Chen, X. Zhang, H. Tian, C. Bao, D. Yan, Y. Geng and F. Wang, *Macromolecules*, 2012, **45**, 8621–8627.
25 S. Ozdemir, M. Sendur, G. Oktem, Ö. Doğan and L. Toppare, *J. Mater. Chem.*, 2012, 22, 4687.
26 E. N. Esmer, S. Tarkuc, Y. A. Udum and L. Toppare, *Mater. Chem. Phys.*, 2011, **131**, 519–524.
27 S. Tarkuc, E. K. Unver, Y. A. Udum and L. Toppare, *Eur. Polym. J.*, 2010, **46**, 2199–2205.
28 K. Takimiya, I. Osaka and M. Nakano, *Chem. Mater.*, 2014, **26**, 587–593.
29 B. Fu, J. Baltazar, A. R. Sankar, P.-H. Chu, S. Zhang, D. M. Collard and E. Reichmanis, *Adv. Funct. Mater.*, 2014, **24**, 3734–3744.
30 Y. Jiang, D. Yu, L. Lu, C. Zhan, D. Wu, W. You, Z. Xie and S. Xiao, *J. Mater. Chem. A*, 2013, **1**, 8270–8279.
31 M. Sendur, A. Balan, D. Baran, B. Karabay and L. Toppare, *Org. Electron.*, 2010, **11**, 1877–1885.
32 H. Shang, H. Fan, Y. Liu, W. Hu, Y. Li and X. Zhan, *Adv. Mater.*, 2011, **23**, 1554–1557.
33 A. Durmus, G. E. Gunbas, P. Camurlu and L. Toppare, *Chem. Commun.*, 2007, 3246.
34 S. Pelz, J. Zhang, I. Kanelidis, D. Klink, L. Hyzak, V. Wulf, O. J. Schmitz, J.-C. Gasse, R. Frahm, A. Pütz, A. Colsmann, U. Lemmer and E. Holder, *European J. Org. Chem.*, 2013, **2013**, 4761–4769.
35 J. Roncali, *Chem. Rev.*, 1992, **92**, 711–738.
36 P. J. Skabara, R. Berridge, I. M. Serebryakov, A. L. Kanibolotsky, L. Kanibolotskaya, S. Gordeyev, I. F. Perepichka, N. S. Sariciftci and C. Winder, *J. Mater. Chem.*, 2007, **17**, 1055–1062.
37 M. Scarongella, A. Laktionov, U. Rothlisberger and N. Banerji, *J. Mater. Chem. C*, 2013, **1**, 2308–2319.
38 B. Fu, J. Baltazar, Z. Hu, A. T. Chien, S. Kumar, C. L. Henderson, D. M. Collard and E. Reichmanis, *Chem. Mater.*, 2012, **24**, 4123–4133.
39 B. Qu, H. Yang, D. Tian, H. Liu, Z. Cong, C. Gao, Z. Chen, L. Xiao, Z. Gao, W. Wei and Q. Gong, *Synth. Met.*, 2012, **162**, 2020–2026.
40 W. Y. Wong, X. Wang, H. L. Zhang, K. Y. Cheung, M. K. Fung, A. B. Djurišić and W. K. Chan, *J. Organomet. Chem.*, 2008, **693**, 3603–3612.
41 G. R. Eaton, S. S. Eaton, D. P. Barr and R. T. Weber, *Quantitative EPR: A practitioners guide*, Springer Vienna, Vienna, 2010.

View Article Online
DOI: 10.1039/C5RA06993A

42 J. Heinze, B. a Frontana-Uribe and S. Ludwigs, *Chem. Rev.*, 2010, **110**, 4724–4771.
43 A. Mirloup, N. Leclerc, S. Rihn, T. Bura, R. Bechara, A. Hébraud, P. Lévêque, T. Heiser and R. Ziessel, *New J. Chem.*, 2014, **38**, 3644–3653.
44 J. Pina, J. S. de Melo, D. Breusov and U. Scherf, *Phys. Chem. Chem. Phys.*, 2013, **15**, 15204–13.
45 E. Ripaud, Y. Olivier, P. Leriche, J. Cornil and J. Roncali, *J. Phys. Chem. B*, 2011, **115**, 9379–9386.
46 Z. Chen, J. Fang, F. Gao, T. J. K. Brenner, K. K. Banger, X. Wang, W. T. S. Huck and H. Sirringhaus, *Org. Electron.*, 2011, **12**, 461–471.
47 J. Y. Lee, S. W. Heo, H. Choi, Y. J. Kwon, J. R. Haw and D. K. Moon, *Sol. Energy Mater. Sol. Cells*, 2009, **93**, 1932–1938.
48 J. Tsutsumi, H. Matsuzaki, N. Kanai, T. Yamada and T. Hasegawa, *J. Phys. Chem. C*, 2013, **117**, 16769–16773.
49 C. Deibe, T. Strobe and V. Dyakonov, *Adv. Mater.*, 2010, **22**, 4097–4111.
50 J. Gierschner, J. Cornil and H.-J. Egelhaaf, *Adv. Mater.*, 2007, **19**, 173–191.
51 I. Osaka, M. Shimawaki, H. Mori, I. Doi, E. Miyazaki, T. Koganezawa and K. Takimiya, *J. Am. Chem. Soc.*, 2012, **134**, 3498–3507.
52 D. Fichou, *Handbook of Oligo- and Polythiophenes*, Wiley-VCH Verlag GmbH, Weinheim, Germany, 1998.
53 T. Nishinaga and K. Komatsu, *Org. Biomol. Chem.*, 2005, **3**, 561.
54 Y. Yu, E. Gunic, B. Zinger and L. L. Miller, *J. Am. Chem. Soc.*, 1996, **118**, 1013–1018.
55 J. L. Bredas and G. B. Street, *Acc. Chem. Res.*, 1985, **18**, 309–315.
56 W. Domagala, B. Pilawa and M. Lapkowski, *Electrochim. Acta*, 2008, **53**, 4580–4590.
57 E. Xu, H. Zhong, J. Du, D. Zeng, S. Ren, J. Sun and Q. Fang, *Dye. Pigment.*, 2009, **80**, 194–198.